Acta Oceanol. Sin., 2023, Vol. 42, No. 12, P. 63–76
https://doi.org/10.1007/s13131-023-2199-1
http://www.aosocean.com
E-mail: ocean2@hyxb.org.cn

Modeling wave attenuation by vegetation with accompanying currents in SWAN

Hong Wang[1, 2], Zhan Hu[1, 3, 4*]

[1] School of Marine Sciences, Sun Yat-Sen University/Southern Marine Science and Engineering Guangdong Laboratory (Zhuhai), Zhuhai 519000, China

[2] State Key Laboratory of Internet of Things for Smart City/Department of Ocean Science and Technology, University of Macau, Macau 999078, China

[3] Guangdong Provincial Key Laboratory of Marine Resources and Coastal Engineering, Guangzhou 510000, China

[4] Pearl River Estuary Marine Ecosystem Research Station, Ministry of Education, Zhuhai 519000, China

Received 15 June 2022; accepted 2 October 2022

Abstract

Coastal wetlands such as salt marshes and mangroves provide important protection against stormy waves. Accurate assessments of wetlands' capacity in wave attenuation are required to safely utilize their protection services. Recent studies have shown that tidal currents have a significant impact on wetlands' wave attenuation capacity, but such impact has been rarely considered in numerical models, which may lead to overestimation of wave attenuation in wetlands. This study modified the SWAN (Simulating Waves Nearshore) model to account for the effect of accompanying currents on vegetation-induced wave dissipation. Furthermore, this model was extended to include automatically derived vegetation drag coefficients, spatially varying vegetation height, and Doppler Effect in combined current-wave flows. Model evaluation against an analytical model and flume data shows that the modified model can accurately simulate wave height change in combined current-wave flows. Subsequently, we applied the new model to a mangrove wetland on Hailing Island in China with a special focus on the effect of currents on wave dissipation. It is found that the currents can either increase or decrease wave attenuation depending on the ratio of current velocity to the amplitude of the horizontal wave orbital velocity, which is in good agreement with field observations. Lastly, we used Hailing Island site as an example to simulate wave attenuation by vegetation under hypothetical storm surge conditions. Model results indicate that when currents are 0.08–0.15 m/s and the incident wave height is 0.75–0.90 m, wetlands' wave attenuation capacity can be reduced by nearly 10% compared with pure wave conditions, which provides implications for critical design conditions for coastal safety. The obtained results and the developed model are valuable for the design and implementation of wetland-based coastal defense. The code of the developed model has been made open source, in the hope to assist further research and coastal management.

Key words: wave attenuation by vegetation, wave-current interaction, SWAN model, storm waves, drag coefficient

Citation: Wang Hong, Hu Zhan. 2023. Modeling wave attenuation by vegetation with accompanying currents in SWAN. Acta Oceanologica Sinica, 42(12): 63–76, doi: 10.1007/s13131-023-2199-1

1 Introduction

In the era of global climate change, storm events form a great threat to the coastal areas (Neumann et al., 2015; Wang et al., 2018). The ability of coastal wetlands (e.g., mangroves and salt marshes) in attenuating wave energy under storm surge conditions has been studied (Loder et al., 2009; Sheng et al., 2012; Möller et al., 2014; Rupprecht et al., 2017; Garzon et al., 2019). They provide valuable services in dissipating wave energy and reducing shoreline erosion (Temmerman et al., 2013; van Loon-Steensma et al., 2014, 2016). Thus, it is proposed to integrate these coastal ecosystems into coastal defense systems as nature-based solutions (Dai and Ge, 2022; Zheng et al., 2023). In the implementation of these solutions, the effectiveness of these systems in attenuating waves in realistic hydrodynamic conditions is critical (Möller et al., 2014).

The process of wave attenuation by vegetation in pure wave conditions has been well studied. Dalrymple et al. (1984) is one of the first studies that assessed wave dissipation by vegetation accounting for the work done by vegetation drag force. The drag force is quantified using Morison equation (Morison et al., 1950). The analytical model of Dalrymple et al. (1984) has been further extended with consideration of random incident waves and wave breaking processes (Mendez and Losada, 2004), which was subsequently implemented in a numerical model, i.e. Simulating Waves Nearshore (SWAN, Suzuki et al., 2012). The SWAN model has been applied in numerous laboratory and field studies to assess the wave height reduction in vegetated fields (Cao et al., 2015; Vuik et al., 2016; Wu et al., 2016; Baron-Hyppolite et al., 2019).

Recent efforts have been made to understand the process of wave dissipation by vegetation in combined current-wave flows,

Foundation item: The National Natural Science Foundation of China under contract No. 42176202; the Innovation Group Project of Southern Marine Science and Engineering Guangdong Laboratory (Zhuhai) under contract No. 311021004; the Guangdong Provincial Department of Science and Technology under contract No. 2019ZT08G090; the 111 Project under contract No. B21018.
*Corresponding author, E-mail: huzh9@mail.sysu.edu.cn

as it is the most common flow condition in natural coastal wetlands. Previous studies have shown an important effect of accompanying tidal currents on wave dissipation by vegetation (Ota et al., 2004; Li and Yan, 2007; Paul et al., 2012; Hu et al., 2014; Losada et al., 2016; Yin et al., 2020; Zhao et al., 2021). It has been revealed that the following currents (i.e., currents flow in the same direction as wave propagation) could either increase or decrease wave dissipation by vegetation depending on the ratio between the current velocity and the amplitude of the horizontal wave orbital velocity (Hu et al., 2014, 2021, 2022; Yin et al., 2020; Zhao et al., 2021). An analytical model has been proposed to explain the different wave dissipation patterns, but the change in wave celerity due to accompanying currents (Doppler Effect) was not considered in the model. Based on large-scale wave basin experiments (Maza et al., 2015; Lara et al., 2016), a new analytical formulation has been developed including the Doppler Effect on wave dissipation in combined current-wave flows (Losada et al., 2016). However, the contribution of currents to vegetation drag force was neglected in such a model. Furthermore, there is a lack of assessable numerical models to estimate wave attenuation by vegetation in combined current-wave flows.

The widely used SWAN vegetation model provides a suitable base to quantify wave dissipation by vegetation with accompanying currents. The main reason is that the wave-current interactions can be readily accounted for in the wave action balance equation, which is the core of the SWAN model. In the current study, we modified the SWAN model to consider the effect of accompanying currents in vegetation-induced wave dissipation, as SWAN-CWV model (i.e., SWAN current-wave-vegetation model). Additionally, to provide a refined modeling tool for field conditions, we further equipped the model with an automatic estimation of vegetation drag coefficients and spatially varying vegetation height to simulate the natural zonation in coastal wetlands (e.g., see Fig. 1a, for details see Section 2). The implementation of the numerical model was validated against a newly-developed analytical model, laboratory data, and field measurements in a mangrove wetland on Hailing Island in China. Subsequently, the SWAN-CWV model was applied to simulate wave energy dissipation under hypothetical storm conditions with coexisting currents, using our measuring transect on Hailing Island as an example. Thus, the current study applied the new SWAN-CWV model to provide a full assessment of the vegetation-induced wave dissipation in storm events. Lastly, the code of the model has been made open source and can be downloaded at https://doi.org/10.6084/m9.figshare.20060291.v1 to assist further research and facilitate the utilization of vegetation wetlands in coastal defense.

2 SWAN-CWV model

The original SWAN model was developed at the Delft University of Technology (http://www.swan.tudelft.nl) to solve the spectral action balance equation. In this study, we developed a modified version of the original SWAN model as SWAN-CWV model. The main modifications are: (1) to include the effects of currents on wave attenuation by vegetation via adding a new term, i.e., $f'(\alpha)$ (see Eqs (10)–(15) below), (2) an automatic estimation of C_D values using an established relation (see Eq. (16) below), and (3) spatially varying vegetation height.

The SWAN is a Eulerian model that quantifies the changes of wave action density spectrum $N(\sigma, \theta)$, which is defined as

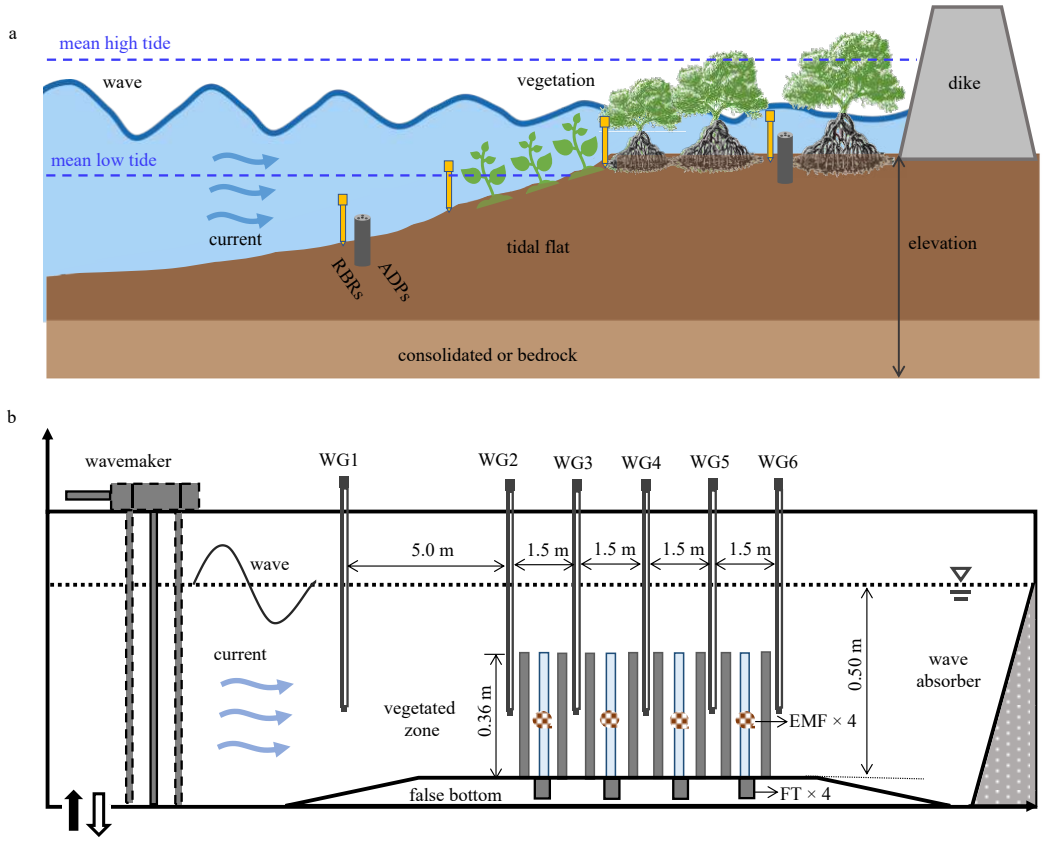

Fig. 1. Wetland ecosystem in combined current-wave flows (a) and wave flume set up (Hu et al., 2014) (b). ADP, RBR, WG, EMF, FT represent Acoustic Doppler Profiler, pressure sensors (RBR solo^3), Wave Gauge, electromagnetic flow meter, and force transducer for measuring parameters of currents and waves.

$$N(\sigma,\theta)=\frac{E(\sigma,\theta)}{\sigma}. \tag{1}$$

The action density $N(\sigma,\theta)$ is defined as the ratio of wave energy density $E(\sigma,\theta)$ and relative frequency σ. N is conserved during propagation along the wave characteristic in the presence of currents. Wave direction θ is an independent variable. The spectral action balance equation can be described in Cartesian co-ordinates as

$$\frac{\partial N}{\partial t}+\frac{\partial c_x N}{\partial x}+\frac{\partial c_y N}{\partial y}+\frac{\partial c_\sigma N}{\partial \sigma}+\frac{\partial c_\theta N}{\partial \theta}=\frac{S_{\rm tot}}{\sigma}, \tag{2}$$

where the first term on the left side represents local change rate of $N(\sigma,\theta)$ over time, as well as the second and third represent the propagation in a coordinate system with velocity c_x and c_y. The fourth term represents the effect of shifting the radian frequency owing to variations in depth and mean currents. The fifth term represents the variation with direction resulting from refraction, where c_σ and c_θ are the propagation velocities in spectral space. $S_{\rm tot}$ on the right side is the source/sink term including wind input $S_{\rm in}$, waves non-linear interactions, e.g., triads $S_{\rm n13}$ and quadruplets $S_{\rm n14}$, waves energy dissipation due to white capping $S_{\rm ds,w}$, bottom friction $S_{\rm ds,b}$, depth-induced wave breaking $S_{\rm ds,br}$ and wave attenuation by vegetation $S_{\rm ds,veg}$, as

$$S_{\rm tot}=S_{\rm in}+S_{\rm n13}+S_{\rm n14}+S_{\rm ds,w}+S_{\rm ds,b}+S_{\rm ds,br}+S_{\rm ds,veg}. \tag{3}$$

To include wave attenuation due to vegetation, Eq. (3) will be extended with $S_{\rm ds,veg}$ (Suzuki et al., 2012). $S_{\rm ds,veg}$ can be extended from a spectral version by considering the property of frequencies and directions (i.e., to have the same form as the other source/sink terms), as

$$S_{\rm ds,veg}(\sigma,\theta)=\frac{D_{\rm tot}}{E_{\rm tot}}E(\sigma,\theta), \tag{4}$$

with

$$D_{\rm tot}=-\frac{1}{2g\sqrt{\pi}}C_{\rm D\_pw}b_{\rm v}N_{\rm v}\left(\frac{\tilde{g}k}{2\tilde{\sigma}}\right)^3\frac{\sinh^3\tilde{k}h_{\rm v}+3\sinh\tilde{k}h_{\rm v}}{3\tilde{k}\cosh^3\tilde{k}h}H_{\rm rms}^3, \tag{5}$$

where g is the acceleration, $C_{\rm D\_pw}$ is the depth-averaged drag coefficient in pure wave conditions, $h_{\rm v}$ is the height of vegetation in water, $b_{\rm v}$ is the stem diameter of vegetation, $N_{\rm v}$ is the number of vegetation per square meter, h is the water depth, $H_{\rm rms}$ is the root-mean-square wave height, $\tilde{\sigma}$ is the mean frequency, $\tilde{k}$ is the mean wave number, and $E_{\rm tot}$ is the total wave energy (The WAMDI Group, 1988; Suzuki et al., 2012). $\tilde{\sigma}$, k, $E_{\rm tot}$ can be described as following:

$$\tilde{\sigma}=\left(E_{\rm tot}^{-1}\int_0^{2\pi}\int_0^{\infty}\frac{1}{\sigma}E(\sigma,\theta){\rm d}\sigma{\rm d}\theta\right)^{-1}, \tag{6}$$

$$\tilde{k}=\left(E_{\rm tot}^{-1}\int_0^{2\pi}\int_0^{\infty}\frac{1}{\sqrt{k}}E(\sigma,\theta){\rm d}\sigma{\rm d}\theta\right)^{-2}, \tag{7}$$

$$E_{\rm tot}=\int_0^{2\pi}\int_0^{\infty}E(\sigma,\theta){\rm d}\sigma{\rm d}\theta. \tag{8}$$

With $H_{\rm rms}^2=8E_{\rm tot}$, the final expression of Eq. (4) reads as

$$S_{\rm ds,veg}(\sigma,\theta)=-\sqrt{\frac{2}{\pi}}g^2C_{\rm D\_pw}b_{\rm v}N_{\rm v}\left(\frac{\tilde{k}}{\tilde{\sigma}}\right)^3\times\frac{\sinh^3\tilde{k}h_{\rm v}+3\sinh\tilde{k}h_{\rm v}}{3\tilde{k}\cosh^3\tilde{k}h}\sqrt{E_{\rm tot}}E(\sigma,\theta). \tag{9}$$

The above-mentioned Eqs (4)–(9) are the formulas used in original SWAN to account for wave dissipation by vegetation in pure wave conditions. In this study, we account for the effects of currents on wave attenuation in the SWAN-CWV model with an additional term $f'(\alpha)$:

$$S'_{\rm ds,veg}=f'(\alpha)S_{\rm ds,veg}(\sigma,\theta). \tag{10}$$

The term $f'(\alpha)$ is based on the analytical model in Hu et al. (2014). It is related to $f(\alpha)=\varepsilon_{\rm cw}/\varepsilon_{\rm pw}$, where $\varepsilon_{\rm pw}$ and $\varepsilon_{\rm cw}$ are the time-averaged rate of energy dissipation per unit horizontal area induced by the vegetation in pure wave and current-wave conditions, respectively (see Eqs (18) and (19) below). In current-wave conditions, Hu et al. (2014) assumes that the instantaneous velocity $u(t)$ equals to $U_{\rm c}+U_{\rm w}\sin(\sigma t)$, where $U_{\rm c}$ and $U_{\rm w}$ are the imposed steady current velocity and the amplitude of horizontal wave orbital velocity. The wave-current angular frequency $\sigma_{\rm wc}$ ($\sigma_{wc}=\sigma-U_{\rm c}k$) is used in the expression of $U_{\rm w}$ to consider the Doppler Effect. Then, $f(\alpha)$ can be derived as following (for details see Hu et al. (2014)):

$$f(\alpha)=\frac{\varepsilon_{\rm cw}}{\varepsilon_{\rm pw}}=\begin{cases}D\dfrac{3}{4}\arcsin(|\alpha|)\left(2|\alpha|\alpha^2+3|\alpha|\right)+\\ \quad\dfrac{1}{4}\left(4+11\alpha^2\right)\left(\sqrt{1-\alpha^2}\right)-\dfrac{3\pi}{4}|\alpha|\alpha^2,\ |\alpha|<1,\\ D\dfrac{9\pi}{8}|\alpha|,\ |\alpha|\geqslant 1,\end{cases} \tag{11}$$

where $D=C_{\rm D\_cw}/C_{\rm D\_pw}$ is the ratio of drag coefficient in current-wave flows and pure wave cases, and it is determined using an empirical relation given in Eq. (16).

Subsequently, $f'(\alpha)$ is obtained based on $f(\alpha)$ following (Hu et al., 2014). This modification is necessary as experiments have shown that the time-mean velocity ($U_{\rm mean}$) is nonzero but in the opposite direction of the wave propagation in pure wave cases due to Stokes drift (Hu et al., 2014, 2022; Chen et al., 2018, 2020), which could affect the quantification of the $\varepsilon_{\rm cw}/\varepsilon_{\rm pw}$ ratio. To account for such effect, Eq. (11) is modified as following:

$$f'(\alpha)=\begin{cases}1,\ \alpha=0,\\ \dfrac{f(\alpha+\gamma_2)}{f(\gamma_1)},\ \alpha>0,\end{cases} \tag{12}$$

where $\gamma_1=U_{\rm mean}/U_{\rm w}$ is determined by averaging the measured ratios in all the pure wave cases in the experimental dataset of Hu et al. (2021). In current-wave cases, $U_{\rm mean}$ is suppressed by the wave motion and thus smaller than the imposed current velocity ($U_{\rm c}$). The value $\gamma_2=U_{\rm mean}/U_{\rm w}-U_{\rm c}/U_{\rm w}$ is determined by averaging the measured ratios in all the current-wave cases in the

above-mentioned dataset. We use the mass transport velocity to calculate the U_{mean}, as follows:

$$U_{\mathrm{mean}} = \frac{H^2k^2}{8}\frac{\cosh 2k\left(z_0+h\right)}{\sinh^2 kh}c, \tag{13}$$

where c is the wave celerity.

The layer schematization due to differences in vertical characteristics of vegetation has been included. The contribution of each vertical segment is calculated individually, and the total energy dissipation equals to the sum of the dissipation in each layer up to the still water level. To add the effects of currents based on Eqs (10)–(13), the final expression of wave attenuation by vegetation of Eq. (4) therefore becomes

$$S'_{\mathrm{ds,veg}} = \sum_{i=1}^{I} S'_{\mathrm{ds,veg},i}, \tag{14}$$

with

$$S'_{\mathrm{ds,veg},i} = -f'\left(\alpha\right)_i\sqrt{\frac{2}{\pi}}g^2C_{\mathrm{D\_pw},i}b_{\mathrm{v},i}N_{\mathrm{v},i}\left(\frac{\widetilde{k}}{\widetilde{\sigma}}\right)^3\times \frac{\left(\sinh^3\widetilde{k}h_{\mathrm{v},i}-\sinh^3\widetilde{k}h_{\mathrm{v},i-1}\right)+3\left(\sinh\widetilde{k}h_{\mathrm{v},i}-\sinh\widetilde{k}h_{\mathrm{v},i-1}\right)}{3k\cosh^3\widetilde{k}h}\times \sqrt{E_{\mathrm{tot}}}E\left(\sigma,\theta\right), \tag{15}$$

where I is the number of vegetation layers, i is the layer under consideration with the energy dissipation for layer i. Compared with the original SWAN model, the flow term $f'\left(\alpha\right)_i$ was incorporated into the expression of wave attenuation $S_{\mathrm{ds,veg},i}$, which considers the effects of accompanying currents.

We further equipped the original SWAN model with an automatic estimation of C_{D} values based on an empirical Re-C_{D} relation proposed in Hu et al. (2014) as following:

$$C_{\mathrm{D}} = 1.04 + \left(\frac{730}{Re}\right)^{1.37}, \quad 300 < Re < 4\,700, \tag{16}$$

where $Re = U_{\mathrm{mid}}b_{\mathrm{v}}/\nu$ is the Reynolds number and $\nu = 10^{-6}$ m^2/s is the kinematic viscosity. U_{mid} equals to U_{w} in the middle of each layer in pure wave conditions or $U_{\mathrm{mean}} + U_{\mathrm{w}}$ in current-wave conditions, respectively. Since this relation is applicable to both pure wave and current-wave cases, Eq. (16) was incorporated in Eq. (15) to calculate the $C_{\mathrm{D\_pw}}$ values as well as in Eq. (11) to calculate the D values ($D = C_{\mathrm{D\_cw}}/C_{\mathrm{D\_pw}}$). Lastly, spatially varying vegetation height (vegetation zonation) in coastal wetlands (see Fig. 1a and Fig. 5b) has also been included in the SWAN-CWV model.

3 Model validation

3.1 *Model validation against a new analytical model*

As a theoretical and numerical validation of the SWAN-CWV model, we developed a new analytical model modified from previous studies (Longuet-Higgins and Stewart, 1961; Mendez and Losada, 2004; Suzuki et al., 2012; Hu et al., 2014; Losada et al., 2016). The main advantage of this new model is the inclusion of (1) Doppler Effect and (2) vegetation drag caused by accompanying currents, which are ignored in the model in Hu et al. (2014) and that in Losada et al. (2016), respectively. This model is developed based on the following assumptions (Losada et al., 2016).

(1) Currents and waves are colinear.

(2) Linear wave theory is applicable.

(3) Current U_{c} is uniform over the water depth and alongshore the vegetation canopy.

(4) Turbulent velocity fluctuations are neglectable.

(5) The drag coefficient is a depth-averaged coefficient in space.

(6) Vegetation motion is neglected, and dissipation is only due to drag force.

(7) Constant water depth.

Following Longuet-Higgins and Stewart (1961), if wave propagates with a current (velocity is U_{c}), energy balance for waves along a vegetation meadow can be expressed as

$$\frac{\partial E\left(c_g+U_{\mathrm{c}}\right)}{\partial x} + S_x\frac{\partial U_{\mathrm{c}}}{\partial x} = -\varepsilon_{\mathrm{cw}}, \tag{17}$$

where $E = (1/8)\rho gH^2$ is the wave energy density, as well as H, c, c_g and S_x are the wave height, wave celerity, wave group velocity and radiation stress, respectively. The subscript x indicates wave propagates along x axis. The first term on the left of Eq. (17) represents the wave energy transfer by the group velocity plus the uniform velocity. The second term represents the work done by the mean velocity U_{c} against the radiation stress $S_x = E\left(2c_g/c - 1/2\right)$ (Longuet-Higgins and Stewart, 1960, 1961), which is a way of waves and current coupling. This term is zero due to the assumption of uniform U_{c}. $\varepsilon_{\mathrm{cw}}$ is the time-average rate of energy dissipation per unit horizontal area induced by the vegetation in combined current-wave flows as

$$\varepsilon_{\mathrm{cw}} = f'\left(\alpha\right)\varepsilon_{\mathrm{pw}}, \tag{18}$$

with

$$\varepsilon_{\mathrm{pw}} = \frac{2}{3\pi}\rho C_{\mathrm{D\_pw}}b_{\mathrm{v}}N_{\mathrm{v}}\left(\frac{kg}{2\sigma}\right)^3\frac{\sinh^3 kh_{\mathrm{v}} + 3\sinh kh_{\mathrm{v}}}{3k\cosh^3 kh}H^3, \tag{19}$$

where $\varepsilon_{\mathrm{pw}}$ is the time-averaged rate of energy dissipation per unit horizontal area induced by the vegetation in pure wave conditions (Mendez and Losada, 2004; Suzuki et al., 2012), ρ is the water density, and $f'\left(\alpha\right)$ is the additional flow term based on Eqs (11)–(13).

To fit the expression of energy dissipation in Eq. (5) for random waves, it is assumed that the waves are narrow-banded in frequency and have the same direction. Random waves are assumed to have a Rayleigh probability density function that is related to root-mean-square wave height H_{rms} (Mendez and Losada, 2004; Losada et al., 2016) as

$$p\left(H\right) = \frac{2H}{H_{\mathrm{rms}}^2\exp\left[-\left(\frac{H}{H_{\mathrm{rms}}}\right)^2\right]}, \tag{20}$$

with

$$H_{\mathrm{rms}}^2 = \int_0^{\infty} H^2p\left(H\right)\mathrm{d}H. \tag{21}$$

Since wave energy is a function of the square mean wave height, the relationship between E and the root-mean-square wave height is as

$$E = (1/8)\rho g H^2 = (1/8)\rho g \int_0^\infty H^2 p(H)\,\mathrm{d}H. \tag{22}$$

Therefore, the differential Eq. (17) can be rewritten as

$$\frac{\partial (1/8)\rho g H_{\mathrm{rms}}^2 (c_g + U_c)}{\partial x} = -f'(\alpha)\frac{1}{2\sqrt{\pi}}\rho C_{\mathrm{D\_pw}} b_v N_v \left(\frac{kg}{2\sigma}\right)^3 \frac{\sinh^3 kh_v + 3\sinh kh_v}{3k\cosh^3 kh} H_{\mathrm{rms}}^3. \tag{23}$$

Due to constant water depth (Assumption (7)), the evolution of H_{rms} in combined current-wave flows can be derived as follows (Dalrymple et al., 1984; Mendez and Losada, 2004):

$$\frac{\partial H_{\mathrm{rms}}^2}{\partial x} = -B_0 H_{\mathrm{rms}}^3, \tag{24}$$

where

$$B_0 = \frac{f'(\alpha)\, C_{\mathrm{D\_pw}} b_v N_v k^2 g^2 (\sinh^3 kh_v + 3\sinh kh_v)}{6\sqrt{\pi}\,(c_g + U_c)\cosh^3 kh}. \tag{25}$$

Solving the differential equation with the boundary condition that the wave height at the starting edge of vegetation field is $H(x=0) = H_{\mathrm{rms},0}$, the wave height along the canopy (at distance x) can be derived as

$$H_{\mathrm{rms}} = \frac{H_{\mathrm{rms},0}}{1 + \beta_{\mathrm{wc}} x}, \tag{26}$$

with

$$\beta_{\mathrm{wc}} = \frac{f'(\alpha)}{3\sqrt{\pi}} C_{\mathrm{D\_pw}} b_v N_v H_{\mathrm{rms},0} \times \frac{k^3 g^2 (\sinh^3 kh_v + 3\sinh kh_v)\sinh(kh)}{\sigma^3 \cosh^2 kh\,(2\sigma kh + \sigma\sinh(2kh) + 2U_c k\sinh(2kh))}, \tag{27}$$

where β_{wc} is related to vegetation drag in current-wave flows for random wave transformation. The other variables are consistent with those in Eq. (5). It should be noted that the wave number k corresponds with the peak period T_p. Note that the new analytical model serves as a first validation of the SWAN-CWV model, but it is not applicable for field conditions, because the measuring transect at the field site is on a slope, which violates the assumption of a constant water depth (Assumption (7)).

To reveal the wave attenuation process, wave height attenuation induced by a unit length of canopies is defined as following (Paul et al., 2012; Hu et al., 2014):

$$\Delta H = \frac{H_0 - H_{\mathrm{out}}}{L}, \tag{28}$$

where H_0 and H_{out} are the wave height at the front and the end of a vegetated area (unit in m), respectively. L is the length of the vegetated area (unit in m). The relative wave height decay r_w (ratio between wave attenuation in current-wave flows and that in pure waves) is defined to assess the effect of accompanying currents on wave attenuation,

$$r_w = \frac{\Delta H_{\mathrm{cw}}}{\Delta H_{\mathrm{pw}}}, \tag{29}$$

where subscript "pw" and "cw" represent pure wave and combined current-wave conditions.

The SWAN-CWV model was validated against the analytical model described in Eqs (26) and (27). To investigate the effect of currents, comparisons with the original SWAN model and an analytical model from Losada et al. (2016) were also carried out. Four runs were conducted for each model, with current velocities of 0 m/s, 0.05 m/s, 0.20 m/s, and 0.30 m/s, respectively. The basic parameters at the input boundary were a constant water depth of h = 0.25 m, a peak wave period of T_p = 1.5 s, and a root mean square wave height of H_{rms} = 0.1 m for a calculation length of 20 m. The vegetation height was 0.36 m to form emergent canopies, the vegetation area per unit height was b_v = 0.002 m, the number of vegetation per unit area was N_v = 239 units/m^2, the bulk vegetation drag coefficient (C_D) was calculated according to the empirical Re-C_D relation in Eq. (16), and the vegetation was present for the entire length for this model validation. A uni-directional narrow-banded random wave was achieved by a Bin frequency spectrum in the SWAN-CWV and SWAN models with a spectrum width of 0.01 and a directional spreading of 2.0°. Wave breaking and bottom friction were not considered in these tests. A 1-D grid with a flat bottom was chosen, and the calculation grid size of the numerical models was set as 1.0 m.

The results of the first validation of the SWAN-CWV model are shown in Fig. 2. Overall, discrepancies among the four models are not apparent in pure wave tests and small current (i.e., 0.05 m/s) tests, except for the analytical model proposed by Losada et al. (2016) (Figs 2a and b). In the pure wave tests, there is a very small difference (within 1.6%) between SWAN-CWV model and SWAN model due to the modification of Eqs (11)–(13). As the current velocity increases to 0.05 m/s, models agree reasonably well with each other. The small difference between SWAN-CWV model and SWAN model in pure waves is eliminated due to the offset of the small currents and the reverse compensation flow. Higher current velocity (i.e., 0.20 m/s and 0.30 m/s) leads to a great difference in modeling results. The SWAN-CWV model is in good agreement with the new analytical model, but the SWAN model underestimates wave attenuation. Furthermore, SWAN-CWV model shows that small currents can suppress wave attenuation by vegetation compared to pure wave case (Fig. 2b), but large currents can enhance wave attenuation, which is in-line with previous studies (Hu et al., 2014; Zhao et al., 2021; Zhang and Nepf, 2021). The analytical model proposed by Losada et al. (2016) is not sensitive to the currents and the wave height decreases linearly while the SWAN-CWV model presents a nonlinear logarithmic decay trend.

3.2 *Model validation with flume experiments*

To further validate the SWAN-CWV model, we tested it against the laboratory experiment data from Hu et al. (2014). The experiment was carried out in a 40-m-long and 0.8-m-wide wave flume in the Fluid Mechanics Laboratory of Delft University of Technology. The vegetation canopy was 6 m long and 0.8 m wide, and the stems were distributed uniformly on the flat bottom. The height of the mimic vegetation was 0.36 m, and the diameter was

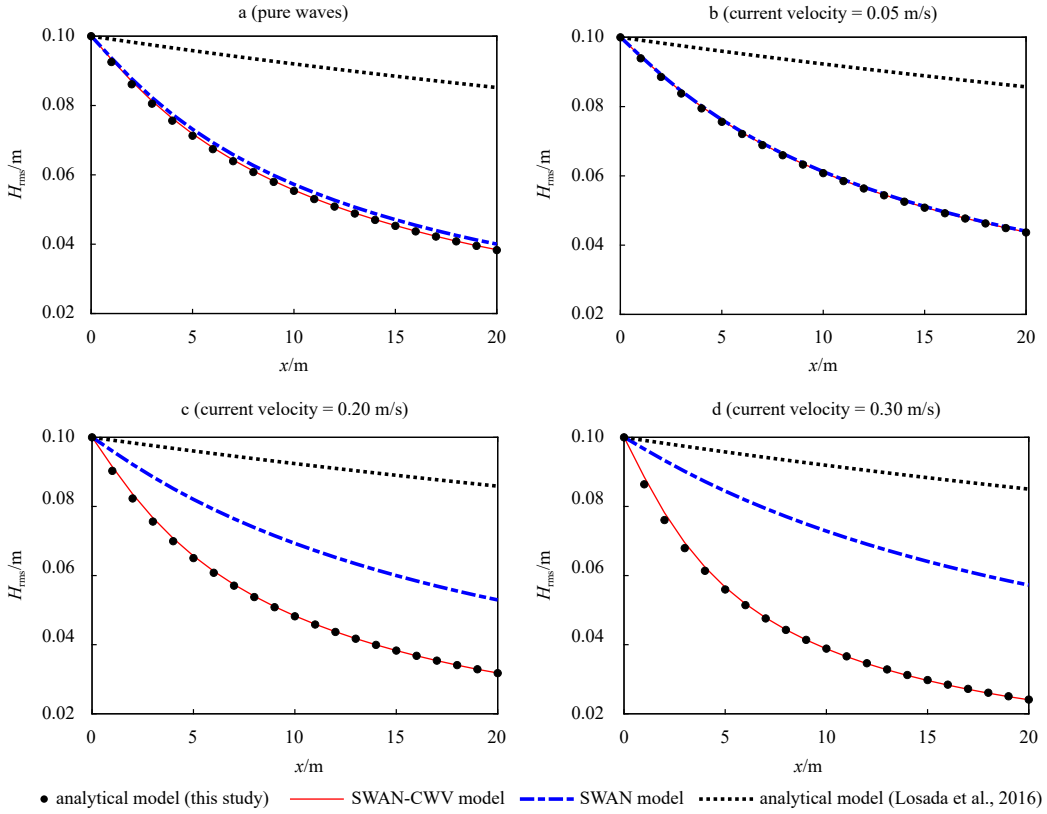

Fig. 2. Comparisons of H_{rms} evolution for SWAN-CWV model with the SWAN model, the analytical model proposed in this study on Eqs (26) and (27), and the analytical model from Losada et al. (2016) with different current velocities. a. Pure waves, b. current velocity = 0.05 m/s, c. current velocity = 0.20 m/s; and d. current velocity = 0.30 m/s. All the tested incident wave height H_{rms} is 0.1 m and the wave period T_p is 1.5 s. The drag coefficients were all calculated according to the empirical Re-C_D relation on Eq. (16) to exclude the influence of C_D to wave attenuation.

0.01 m. Water depths of 0.25 m and 0.50 m were chosen to achieve emergent and submerged canopies. The vegetation bulk drag coefficient was decided by Reynolds number, as shown in Eq. (16). A detailed analysis of the flume experiment can be found in Hu et al. (2014). In total, 238 tests were conducted with three different vegetation densities (VD0, VD1, VD2), two water depths, and various wave-current conditions (Table A1 in Appendix A). Control tests with no vegetation were carried out in the flume to measure the wave height reduction by bottom friction of the flume bed and sidewalls (VD0).

To reveal the importance of currents in the modeling, we developed an additional SWAN-C_D model as a comparison to the SWAN-CWV model. The former does not consider the effect of currents on wave attenuation, but still accounts for changing C_D according to Eq. (16). Uni-directional regular waves in SWAN-CWV and SWAN-C_D were achieved by setting a spectrum width of 0.01 and a directional spreading of 2°. The breaking function and friction function were not used in these cases. A 1-D grid was used to reproduce the central line of the plant canopy. The calculation grid size of the SWAN-CWV model and SWAN-C_D model was set as 1.0 m. The current velocity at the edge of the canopy was chosen to represent the flow state in the whole vegetation area (Maza et al., 2015). Besides, an additional sensitivity analysis of different grid sizes (1 m, 2 m and 5 m) on the SWAN-CWV simulating results were carried out (Fig. B1 in Appendix B).

An example of this model validation shows that the SWAN-CWV model can well reproduce the wave height attenuation in combined current-wave flows (Fig. 3). As a contrast, the SWAN-

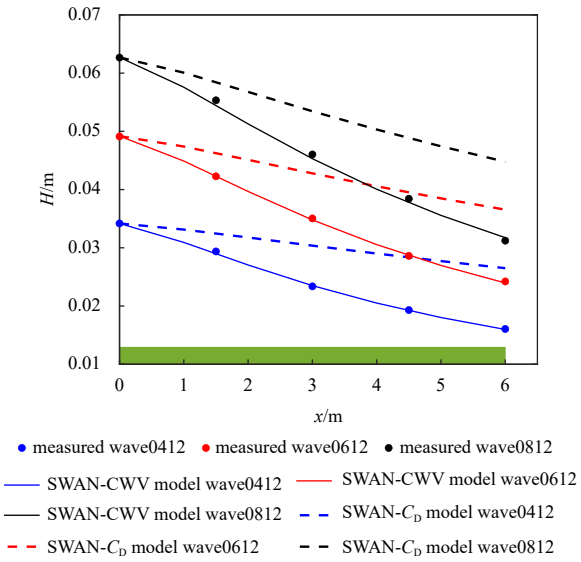

Fig. 3. Comparisons of the wave height along mimic canopies (green patch) in the current-wave flows (U_c = 0.20 m/s): SWAN-CWV, SWAN-C_D and the measured data (Hu et al., 2014). All cases are in non-submerged canopies with medium mimic stem densities (139 stems/m^2). The case name stands for the combination of incident wave height 0.04 m and wave period 1.2 s, namely wave0412.

C_D model (only considers C_D variations but does not consider the effect of current) has a clear underestimation trend for wave attenuation. In the three cases, the wave height reduction is close to 45% from the SWAN-CWV model while less than 30% from the SWAN-C_D model. Such a difference can systematically reveal the effect of accompanying currents on wave dissipation by vegetation.

The SWAN-CWV model was further applied to simulate wave height changes in various flow and vegetation density conditions that were tested in Hu et al. (2014) (Fig. 4). The simulations were classified into two groups according to α ($\alpha = U_c/U_w$). They show that the SWAN-CWV model performs better than the SWAN-C_D model in both groups. When α is less than 1, the coefficient of determination (R^2) of the SWAN-CWV model outputs ($\Delta H = (H_0 - H_{out})/L$) is 0.84, and the bias is 0.05. The R^2 simulated by the SWAN-C_D model is 0.70, and the bias is 0.15. When α is greater than 1, the R^2 of the SWAN-CWV model outputs is 0.76, while the R^2 of the SWAN-C_D model outputs reduces to 0.36.

3.3 *Model validation with field observations*

An application of the SWAN-CWV model to a field site was conducted. The field measurements were carried out on Hailing Island located in the Shenqian Bay, a large coastal embayment in the south of China (Fig. 5a). The mangrove communities are dominated by the *Aegiceras corniculatum* and *Kandelia candel,* with a stem diameter of 0.06–0.12 m. The local mean tidal range is 2.5 m. The maximum tide range can reach 3 m, and the minimum tide range is 0.5 m.

Four stations were set up at the field site to measure wave height and water depth, and two of these stations (S1 and S4 in Fig. 5b) were also used to measure tidal current velocity. The stations were deployed along a transect through bare flat, seedling zone, and mature mangroves, with a length of 70 m. The mature mangrove vegetation area was 20 m, the seedling area was 35 m, and the bare land was 15 m. Vegetation height, diameter, and density were measured and varied between 0.4–2.0 m, 0.02–0.20 m, and 1–10 stems/m^2, respectively (Table 1). The elevation of the observation profile ranged from 0.05 m to 0.38 m, with the mean sea level at 0 m. The elevation of Stations S1, S2, S3 and S4 relative to the mean sea level were 0.33 m, 0.32 m, 0.29 m and 0.19 m, respectively.

The measurements were conducted during December 10–29, 2018. Wave parameters, including the significant wave heights (H_s), wave periods (T_p), and the water depths were measured using pressure sensors (RBR solo^3, Fig. 5d). Current velocity was measured using Nortek Acoustic Doppler Profile (ADP) instruments, which were placed in holes on the seabed with upward-looking measuring heads (Fig. 5c). The measuring interval of the velocity profile was 10 min (for details about instrument settings see Hu et al. (2020)). The bathymetry data were collected by an real-time kinematic (RTK) survey, which were subsequently used as model inputs. Vegetation characters were obtained by averaging four 5 m × 5 m grids in each zone.

The grid size of the model was set as 5.0 m. The incident wave spectrum at the seaward boundary has a JONSWAP spectrum with a spectral peak parameter of 3.3. The frequency range of the spectrum was 0.1–4.0 Hz and the resolution was 0.1 Hz. The direction range of the spectrum was −30° to 30°. The friction-in-

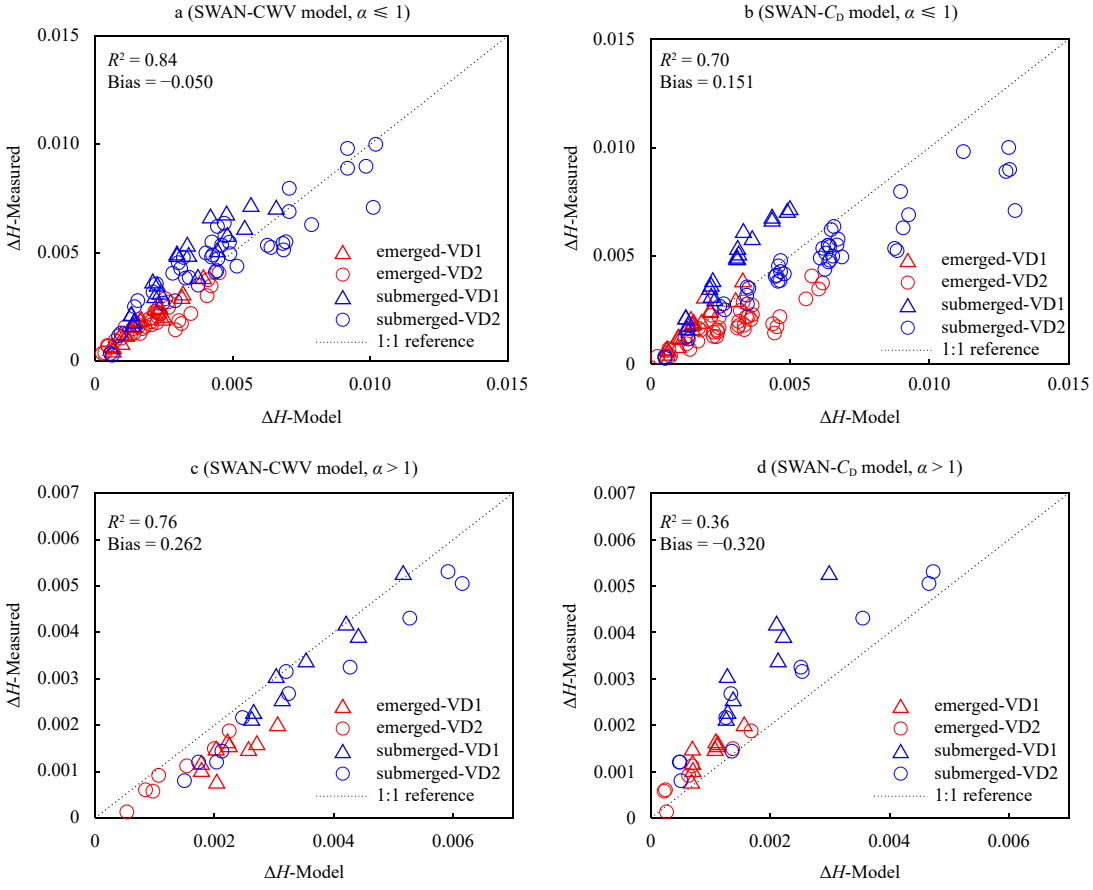

Fig. 4. Comparisons of wave height attenuation induced by a unit length of canopies (ΔH in Eq. (28)) between numerical models (SWAN-CWV and SWAN-C_D) and experiment data (Hu et al., 2014).

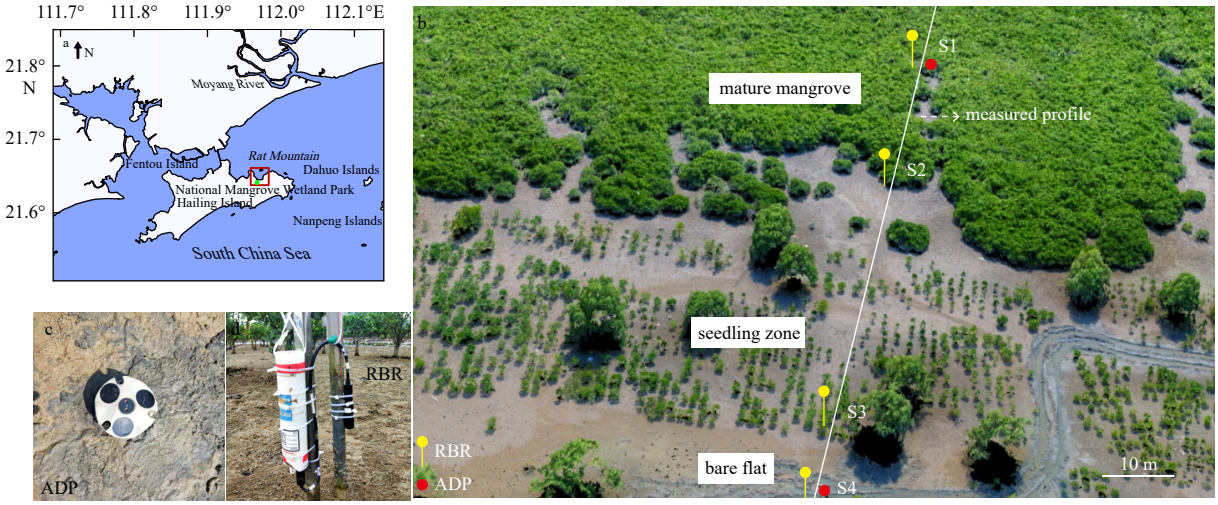

Fig. 5. The study area (enclosed by the red rectangle) on Hailing Island, South of China (a), top view of the study area (b), and ADP (c) and RBR (d) for current and wave measurements, respectively. S1–S4 represent the four stations set up at the field site for measuring wave and current parameters.

Table 1. Input parameters of vegetation characters

Region	Vegetation character				
	Length (x)/m	Height (h_v)/m	Diameter (b_v)/m	Density (N_v)/(stem·m^{-2})	Drag coefficient (C_D)
Mudflat	15	0	0	0	0
Seedling zone	35	0.6	0.05	6	Re-C_D
Mature mangrove	20	1.8	0.15	2	Re-C_D

duced wave attenuation at the bottom of the tidal flat was considered. JONSWAP with a constant friction coefficient 0.038 m^2/s^3 was activated. Furthermore, to better quantify the effect of currents in wave attenuation by vegetation, we tested different numerical models, i.e., original SWAN with a constant C_D = 1.2, SWAN-C_D and SWAN-CWV respectively. As described in Section 2, the vegetation drag coefficient was calculated according to Eq. (16) in the SWAN-C_D model. Furthermore, sensitivity analysis of different grid sizes (1 m, 5 m, and 10 m) on the SWAN-CWV simulating results were also carried out (Fig. B2 in Appendix B).

We compared the wave evolution in SWAN-CWV model, SWAN-C_D model with field observations during December 10–29, 2018, in Hailing Island (Fig. 6). Specifically, we designate currents that flow in the same direction as wave propagation (e.g., flooding currents) as positive currents, and currents that flow in the opposite direction as wave propagation (e.g., ebb currents) as negative currents. The measured incident wave height was between 0 and 0.32 m, and the current velocity ranged from –0.52 m/s to 0.21 m/s in Station S1 during this period. Results show that the observed wave height variation pattern can be well captured by both SWAN-CWV model and SWAN-C_D model with the same (R^2 = 0.97). The bias of the SWAN-CWV model is –0.016 m, while the SWAN-C_D model is 0.045 m (Fig. 6a). When the absolute value of current velocity is greater than 0.20 m/s (i.e., three shaded parts in Fig. 6c), the SWAN-CWV model captures the strong wave attenuation to almost zero. However, the SWAN-C_D model underestimates the wave attenuation.

To systematically compare different models, the simulations of the wave attenuation in field conditions were also classified into different groups according to α ($\alpha = U_c/U_w$). Cases with water depth greater than 0.15 m and the incident wave height over 0.03 m at Station S4 were considered valid cases, with a total of 794. Furthermore, the SWAN model with a constant drag coefficient of 1.2 was also carried out to simulate the cases as a reference to exclude the effect of varying C_D. Results show a discrepancy among the three numerical models is not very apparent when α is smaller than 1, while as the increase of α, their discrepancy becomes larger (Fig. 7). The R^2 values of these three models are the same as 0.97 when α is smaller than 0.25, i.e., in cases with no currents or very weak currents. With the increase of α ($1 \leqslant \alpha \leqslant 1.5$), the R^2 values remain above 0.60 for all the three models. When α is over 1.5, which represents the vegetation is exposed to relatively strong currents, the SWAN-CWV model performs better than the SWAN and the SWAN-C_D models, with the R^2 value apparently higher than the other two models.

4 Modeling wave attenuation by vegetation under hypothetical storm conditions

In this section, we applied the validated SWAN-CWV model to reveal the impact of currents on wave attenuation by vegetation during hypothetical storm conditions. The Hailing Island site in Section 3.3 is considered as an exemplary system. A 1-D rectilinear computational grid with a constant grid size of 5 m was generated for the observation transect. The incident waves come from the seaward boundary, and the landward side was a closed boundary with no wave reflection. The topography and vegetation inputs were adapted from Section 3.3. Storm surge scenarios were set following Möller et al. (2014) with a constant water depth of 2 m. The wave height was set at 0.50 m to 0.90 m, and the wave period was 4.0 s with a following (propagating in the same direction) uniform current velocity of 0 m/s to 0.50 m/s. The JONSWAP spectrum with a peak parameter of 3.3 was selected for the incident wave spectrum. In total, the SWAN-CWV model was applied in 112 tests with different combinations of hydrodynamics, with the aim to reveal the effect of tidal currents.

Both pure wave and combined wave-current cases were

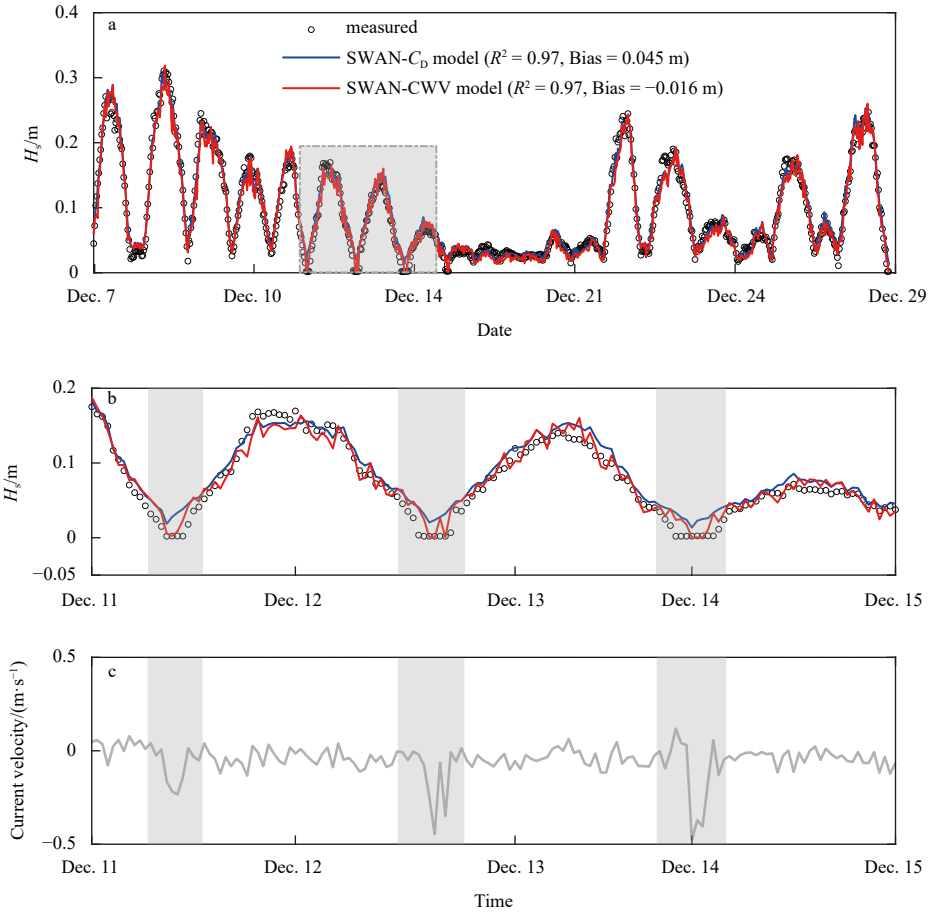

Fig. 6. Comparisons between measured significant wave height in the mature mangroves and results from SWAN-C_D and SWAN-CWV models for field observations in Hailing Island (a and b), and variation of depth-averaged current velocity at Station S1 (c). The shaded area in a is enlarged in b to better show the influence of currents to wave vegetation. Three shaded parts in b represent relatively strong current in the observed period.

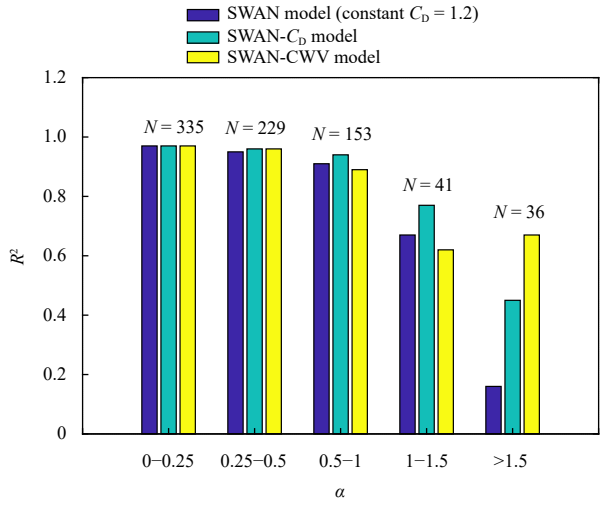

Fig. 7. Statistical results of R^2 for numerical models (SWAN-C_D = 1.2, SWAN-C_D, SWAN-CWV) simulated results according to velocity ratio α ($\alpha = U_c/U_w$) in the field observations.

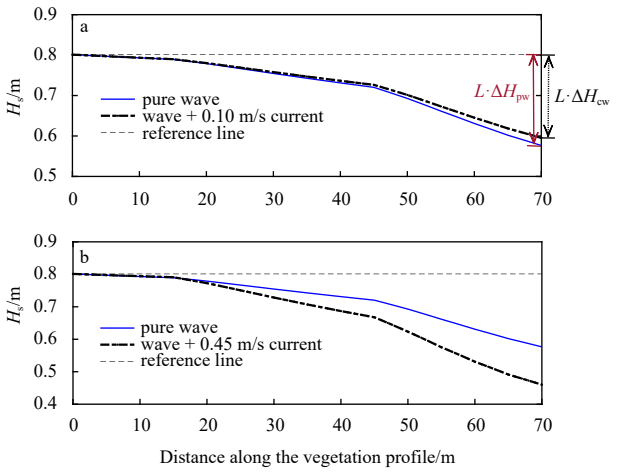

Fig. 8. Variation of the significant wave height along with the canopy in different combinations of waves and currents. a. Weak current (H_0 = 0.8 m, T_p = 4.0 s, U_c = 0.10 m/s); b. strong current (H_0 = 0.8 m, T_p = 4.0 s, U_c = 0.45 m/s). The numerical test in pure wave conditions with the same incident waves was carried out as a reference to assess the currents to wave attenuation (blue line). L is the length of the vegetated area. ΔH_{pw} and ΔH_{cw} stand for the wave height attenuation induced by a unit length of canopies for pure wave and combined current-wave flows in Eq. (28).

tested (Fig. 8). It is shown that the currents can increase or decrease the wave attenuation by vegetation with different wave-current combinations. With the same incident significant wave height of 0.8 m and wave period of 4.0 s, when the current velo-

city is small (i.e., 0.10 m/s), the wave attenuation (ΔH_{cw}) is suppressed by 8.4% compared to the pure wave cases (ΔH_{pw}) (Fig. 8a). However, when the current velocity is higher (i.e., 0.45 m/s), the wave attenuation (ΔH_{cw}) is promoted compared to the pure wave cases (ΔH_{pw}).

With the changing stormy waves and the accompanying tidal currents, the relative wave height decay (r_w) varies greatly from 0.9 to 2.5 (Fig. 9). For the cases with relatively small currents (i.e., 0.08–0.15 m/s) and the incident wave height of 0.80 m, the amount of vegetation-induced wave height reduction is decreased by nearly 10% compared to pure wave conditions (Area I in Fig. 9). However, with the same wave conditions, the wave attenuation by vegetation is increased when the currents become stronger. The cases with stronger currents velocity (i.e., 0.40–0.50 m/s) have nearly 1.5 times higher r_w than pure wave conditions (Area II in Fig. 9). Therefore, the currents can either increase or decrease the wave attenuation by vegetation depending on the different wave and current combinations.

5 Discussion and conclusions

5.1 *Towards accurate modeling of wave dissipation by vegetation with accompanying currents*

Previous studies have revealed large variability in vegetation-induced wave attenuation with the impact of accompanying currents (Li and Yan, 2007; Paul et al., 2012; Hu et al., 2014, 2022; Losada et al., 2016; Zhao et al., 2021; Zhang and Nepf, 2021). An accurate modeling tool is needed to precisely assess wave attenuation in various flow conditions. Two new models have been successfully developed in the current study, i.e., a new numerical model (i.e., SWAN-CWV model) and a new analytical model. These two models were in good agreement with each other as they are developed based on the same core process, although the applied equations were in different forms. The main differences between these two models and the model of Losada et al. (2016) are: (1) the contribution of the current velocity to the drag force, (2) the attribution of Stokes drift, i.e., non-zero mean velocity in pure wave conditions and suppressed current due to wave motion in current-wave conditions (Hudspeth and Sulisz, 1991; Hu et al., 2014; Chen et al., 2020). Compared to the model of Hu et al. (2014), the main advantage of the two new models is the inclusion of the Doppler Effect.

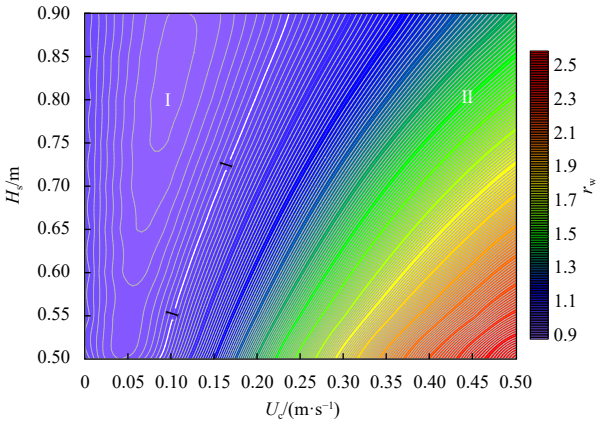

Fig. 9. Variation of r_w ($r_w = \Delta H_{cw}/\Delta H_{pw}$) with different hydrodynamic combinations under the storm surge. The white solid line represents contour 1 ($r_w = 1$), indicating that the wave attenuation caused by vegetation has neither increased nor decreased in the combined current-wave flows compared to the pure wave conditions. Area I indicates a decrease in the amount of vegetation-induced wave height reduction. Area II indicates an increase in wave attenuation by vegetation when the currents become stronger under the same wave conditions.

In addition, we equipped the SWAN-CWV model with an automatic estimation of C_D values based on an empirical Re-C_D relation in Eq. (16). The possibility of horizontal variation of the vegetation height has also been included to reflect the natural zonation in coastal wetlands. The good agreement between the model simulated results and the observation from both laboratory and field shows that the SWAN-CWV model is reliable for wave field simulation of coastal wetlands under combined current-wave conditions. We have made the SWAN-CWV model code open-source at https://doi.org/10.6084/m9.figshare.20060291.v1, in the hope that this numerical tool can assess the research and utilization of the coastal wetlands' defense values.

The SWAN-CWV model still has some limitations and needs further improvements. Firstly, due to the assumption that currents and waves are colinear, the model is not applicable under the conditions of wave-current with an angle. Secondly, it cannot assess current-induced wave breaking in a vegetation field, which is likely to occur with opposing currents (Hu et al., 2022). Lastly, our model regards the vegetation as rigid cylinders, but its flexibility is not considered. If flexible vegetation is under consideration (i.e., marshes and seagrass meadows), this model might not accurately reproduce the wave decay since vegetation stiffness is reduced and the buoyancy is high (Mendez and Losada, 2004; Lara et al., 2016; Losada et al., 2016; Zhang et al., 2021).

5.2 *The effect of vegetation species and discontinuousness on wave attenuation*

Previous studies have revealed that the zonation of the coastal vegetation plays an important role during extreme natural events (Tanaka, 2009; Tanaka et al., 2011; Vandenbruwaene et al., 2011; Yang et al., 2015; Yang and Irish, 2018; Zainali et al., 2018; Zhang et al., 2022). A combination of different tree species is recommended in a buffer forest. Active forest management for the forest age, density, diameter, and stand structure of trees is required to enhance the potential for coastal defense (Tanaka, 2009; Zhao et al., 2020; Zhou et al., 2022). Furthermore, the distribution of the coastal wetlands is also significant in affecting the flow patterns. The wave-induced flow in wetlands has complex circulation characteristics because of the interaction between waves and vegetation, especially in areas with discontinuous patches (Yang et al., 2015).

In the current study, the buffering behavior of mangroves has been examined in the application in Hailing Island. The mangroves are dominated by *Aegiceras corniculatum* and *Kandelia candel* species. Due to different afforestation times, the spatial distribution of vegetation shows different wave dissipating abilities. Our modeling results show that the mature mangrove forests' wave dissipation capacity is nearly three times that of young seedlings in the site, which fit well with the observations. This shows our model is competent in providing wave field assessment, provided that the information on the morphology of mangrove forests is available.

5.3 *Changes in vegetation wave dissipation capacity in storm conditions*

Several studies have already demonstrated the ability of coastal wetlands to efficiently attenuate wave energy during storm surges (Loder et al., 2009; Sheng et al., 2012; Zhao and

Chen, 2014; Rupprecht et al., 2017; Hoque et al., 2018; Garzon et al., 2019). The vegetation flexibility and height, wave conditions and water depth, play an important role in vegetation-waves interaction (Rupprecht et al., 2017). Recent research indicates that the local attenuation of extreme water levels within wetland areas is more effective when the vegetation patches are wider and vegetation resistance is higher (De Dominicis et al., 2023).

This study demonstrates that considering vegetation-induced wave attenuation, the accompanying currents are important factors to be considered in coastal wetlands' wave attenuation capacity. For a specific setup in Hailing Island, modeling results indicate that the currents can increase wave attenuation by vegetation in most cases, but a more alarming note is that when the currents are 0.08–0.15 m/s and the incident wave height is 0.75–0.90 m, the amount of vegetation-induced wave height reduction is decreased by nearly 10% compared with pure wave conditions. In contrast, the previous wave models may overestimate vegetation-induced wave attenuation due to the exclusion of tidal currents. Although this reduction in vegetation-induced wave height reduction may vary at different sites, our modeling results provide a key reference to coastal managers in determining the size of coastal wetlands to sufficiently protect the coasts from storms.

Acknowledgements

The authors would like to thank the members of M5 (Mudflat, Marsh, Mangrove, Measurement & Modeling) Lab at Sun Yat-Sen University for their assistance in the field experimental works.

References

Baron-Hyppolite C, Lashley C H, Garzon J, et al. 2019. Comparison of implicit and explicit vegetation representations in SWAN hindcasting wave dissipation by coastal wetlands in Chesapeake Bay. Geosciences, 9(1): 8, doi: 10.3390/geosciences9010008

Cao Haijin, Feng Weibing, Hu Zhan, et al. 2015. Numerical modeling of vegetation-induced dissipation using an extended mild-slope equation. Ocean Engineering, 110: 258–269, doi: 10.1016/j.oceaneng.2015.09.057

Chen Ming, Lou Sha, Liu Shuguang, et al. 2020. Velocity and turbulence affected by submerged rigid vegetation under waves, currents and combined wave-current flows. Coastal Engineering, 159: 103727, doi: 10.1016/j.coastaleng.2020.103727

Chen Hui, Ni Yan, Li Yulong, et al. 2018. Deriving vegetation drag coefficients in combined wave-current flows by calibration and direct measurement methods. Advances in Water Resources, 122: 217–227, doi: 10.1016/j.advwatres.2018.10.008

Dai Zhijun, Ge Zhenming. 2022. Research and Practice of Green Ecological Coastal Defense. Beijing: Science Press, 104–130

Dalrymple R A, Kirby J T, Hwang P A. 1984. Wave diffraction due to areas of energy dissipation. Journal of Waterway, Port, Coastal, and Ocean Engineering, 110(1): 67–79

De Dominicis M, Wolf J, van Hespen R, et al. 2023. Mangrove forests can be an effective coastal defence in the Pearl River Delta, China. Communications Earth & Environment, 4(1): 13, doi: 10.1038/s43247-022-00672-7

Garzon J L, Maza M, Ferreira C M, et al. 2019. Wave attenuation by *Spartina* saltmarshes in the Chesapeake Bay under storm surge conditions. Journal of Geophysical Research: Oceans, 124(7): 5220–5243, doi: 10.1029/2018JC014865

Hoque A, Husrin S, Oumeraci H. 2018. Laboratory studies of wave attenuation by coastal forest under storm surge. Coastal Engineering Journal, 60(2): 225–238, doi: 10.1080/21664250.2018.1486268

Hu Zhan, Lian Simei, Wei Huaiyu, et al. 2021. Laboratory data on wave propagation through vegetation with following and opposing currents. Earth System Science Data, 13(10): 4987–4999, doi: 10.5194/essd-13-4987-2021

Hu Zhan, Lian Simei, Zitman T, et al. 2022. Wave breaking induced by opposing currents in submerged vegetation canopies. Water Resources Research, 58(4): e2021WR031121, doi: 10.1029/2021WR031121

Hu Zhan, Suzuki T, Zitman T, et al. 2014. Laboratory study on wave dissipation by vegetation in combined current-wave flow. Coastal Engineering, 88: 131–142, doi: 10.1016/j.coastaleng.2014.02.009

Hu Zhan, Zhou Juanling, Wang Chen, et al. 2020. A novel instrument for bed dynamics observation supports machine learning applications in mangrove biogeomorphic processes. Water Resources Research, 56(7): e2020WR027257, doi: 10.1029/2020WR027257

Hudspeth R T, Sulisz W. 1991. Stokes drift in two-dimensional wave flumes. Journal of Fluid Mechanics, 230: 209–229, doi: 10.1017/S0022112091000769

Lara J L, Maza M, Ondiviela B, et al. 2016. Large-scale 3-D experiments of wave and current interaction with real vegetation. Part 1: Guidelines for physical modeling. Coastal Engineering, 107: 70–83, doi: 10.1016/j.coastaleng.2015.09.012

Li C W, Yan K. 2007. Numerical investigation of wave-current-vegetation interaction. Journal of Hydraulic Engineering, 133(7): 794–803, doi: 10.1061/(ASCE)0733-9429(2007)133:7(794

Loder N M, Irish J L, Cialone M A G, et al. 2009. Sensitivity of hurricane surge to morphological parameters of coastal wetlands. Estuarine, Coastal and Shelf Science, 84(4): 625–636

Longuet-Higgins M S, Stewart R W. 1960. Changes in the form of short gravity waves on long waves and tidal currents. Journal of Fluid Mechanics, 8(4): 565–583, doi: 10.1017/S0022112060000803

Longuet-Higgins M S, Stewart R W. 1961. The changes in amplitude of short gravity waves on steady non-uniform currents. Journal of Fluid Mechanics, 10(4): 529–549, doi: 10.1017/S0022112061000342

Losada I J, Maza M, Lara J L. 2016. A new formulation for vegetation-induced damping under combined waves and currents. Coastal Engineering, 107: 1–13, doi: 10.1016/j.coastaleng.2015.09.011

Maza M, Lara J L, Losada I J, et al. 2015. Large-scale 3-D experiments of wave and current interaction with real vegetation. Part 2: Experimental analysis. Coastal Engineering, 106: 73–86, doi: 10.1016/j.coastaleng.2015.09.010

Mendez F J, Losada I J. 2004. An empirical model to estimate the propagation of random breaking and nonbreaking waves over vegetation fields. Coastal Engineering, 51(2): 103–118, doi: 10.1016/j.coastaleng.2003.11.003

Möller I, Kudella M, Rupprecht F, et al. 2014. Wave attenuation over coastal salt marshes under storm surge conditions. Nature Geoscience, 7(10): 727–731, doi: 10.1038/NGEO2251

Morison J R, Johnson J W, Schaaf S A. 1950. The force exerted by surface waves on piles. Journal of Petroleum Technology, 2(5): 149–154, doi: 10.2118/950149-g

Neumann J E, Emanuel K A, Ravela S, et al. 2015. Risks of coastal storm surge and the effect of sea level rise in the Red River Delta, Vietnam. Sustainability, 7(6): 6553–6572, doi: 10.3390/su7066553

Ota T, Kobayashi N, Kirby J T. 2004. Wave and current interactions with vegetation. In: Coastal Engineering 2004. Lisbon, Portugal: World Scientific, 508–520, doi: 10.1142/9789812701916_0040

Paul M, Bouma T J, Amos C L. 2012. Wave attenuation by submerged vegetation: Combining the effect of organism traits and tidal current. Marine Ecology Progress Series, 444: 31–41, doi: 10.3354/meps09489

Rupprecht F, Möller I, Paul M, et al. 2017. Vegetation-wave interactions in salt marshes under storm surge conditions. Ecological Engineering, 100: 301–315, doi: 10.1016/j.ecoleng.2016.12.030

Sheng Y P, Lapetina A, Ma Gangfeng. 2012. The reduction of storm surge by vegetation canopies: Three-dimensional simulations. Geophysical Research Letters, 39(20): L20601, doi: 10.1029/2012GL053577

Suzuki T, Zijlema M, Burger B, et al. 2012. Wave dissipation by vegetation with layer schematization in SWAN. Coastal Engineering, 59(1): 64–71, doi: 10.1016/j.coastaleng.2011.07.006

Tanaka N. 2009. Vegetation bioshields for tsunami mitigation: review of effectiveness, limitations, construction, and sustainable management. Landscape and Ecological Engineering, 5(1): 71–79, doi: 10.1007/s11355-008-0058-z

Tanaka N, Jinadasa K B S N, Mowjood M I M, et al. 2011. Coastal vegetation planting projects for tsunami disaster mitigation: effectiveness evaluation of new establishments. Landscape and Ecological Engineering, 7(1): 127–135, doi: 10.1007/s11355-010-0122-3

Temmerman S, Meire P, Bouma T J, et al. 2013. Ecosystem-based coastal defence in the face of global change. Nature, 504(7478): 79–83, doi: 10.1038/nature12859

The WAMDI Group. 1988. The WAM model—A third generation ocean wave prediction model. Journal of Physical Oceanography, 18(12): 1775–1810, doi: 10.1175/1520-0485(1988)018<1775:TWMTGO>2.0.CO;2

Vandenbruwaene W, Temmerman S, Bouma T J, et al. 2011. Flow interaction with dynamic vegetation patches: Implications for biogeomorphic evolution of a tidal landscape. Journal of Geophysical Research: Earth Surface, 116(F1): F01008, doi: 10.1029/2010JF001788

van Loon-Steensma J M, Hu Zhan, Slim P A. 2016. Modelled impact of vegetation heterogeneity and salt-marsh zonation on wave damping. Journal of Coastal Research, 32(2): 241–252, doi: 10.2112/JCOASTRES-D-15-00095.1

van Loon-Steensma J M, Slim P A, Decuyper M, et al. 2014. Salt-marsh erosion and restoration in relation to flood protection on the Wadden Sea barrier island Terschelling. Journal of Coastal Conservation, 18(4): 415–430, doi: 10.1007/s11852-014-0326-z

Vuik V, Jonkman S N, Borsje B W, et al. 2016. Nature-based flood protection: The efficiency of vegetated foreshores for reducing wave loads on coastal dikes. Coastal Engineering, 116: 42–56, doi: 10.1016/j.coastaleng.2016.06.001

Wang Jun, Yi Si, Li Mengya, et al. 2018. Effects of sea level rise, land subsidence, bathymetric change and typhoon tracks on storm flooding in the coastal areas of Shanghai. Science of the Total Environment, 621: 228–234, doi: 10.1016/j.scitotenv.2017.11.224

Wu Weicheng, Ma Gangfeng, Cox D T. 2016. Modeling wave attenuation induced by the vertical density variations of vegetation. Coastal Engineering, 112: 17–27, doi: 10.1016/j.coastaleng.2016.02.004

Yang Yongqian, Irish J L. 2018. Evolution of wave spectra in mound-channel wetland systems. Estuarine, Coastal and Shelf Science, 207: 444–456, doi: 10.1016/j.ecss.2017.06.012

Yang Yongqian, Irish J L, Socolofsky S A. 2015. Numerical investigation of wave-induced flow in mound-channel wetland systems. Coastal Engineering, 102: 1–12, doi: 10.1016/j.coastaleng.2015.05.002

Yin Zegao, Wang Yanxu, Liu Yong, et al. 2020. Wave attenuation by rigid emergent vegetation under combined wave and current flows. Ocean Engineering, 213: 107632, doi: 10.1016/j.oceaneng.2020.107632

Zainali A, Marivela R, Weiss R, et al. 2018. Numerical simulation of nonlinear long waves in the presence of discontinuous coastal vegetation. Marine Geology, 396: 142–149, doi: 10.1016/j.margeo.2017.08.001

Zhang Wei, Ge Zhenming, Li Shihua, et al. 2022. The role of seasonal vegetation properties in determining the wave attenuation capacity of coastal marshes: implications for building natural defenses. Ecological Engineering, 175: 106494, doi: 10.1016/j.ecoleng.2021.106494

Zhang Xiaoxia, Lin Pengzhi, Nepf H. 2021. A simple-wave damping model for flexible marsh plants. Limnology and Oceanography, 66(12): 4182–4196, doi: 10.1002/lno.11952

Zhang Xiaoxia, Nepf H. 2021. Wave damping by flexible marsh plants influenced by current. Physical Review Fluids, 6(10): 100502, doi: 10.1103/PhysRevFluids.6.100502

Zhao Haihong, Chen Qin. 2014. Modeling attenuation of storm surge over deformable vegetation: methodology and verification. Journal of Engineering Mechanics, 140(12): 04014090, doi: 10.1061/(ASCE)EM.1943-7889.0000704

Zhao Chuyan, Tang Jun, Shen Yongming, et al. 2021. Study on wave attenuation in following and opposing currents due to rigid vegetation. Ocean Engineering, 236: 109574, doi: 10.1016/j.oceaneng.2021.109574

Zhao Chuyan, Zhang Yan, Tang Jun, et al. 2020. Numerical investigation of solitary wave run-up attenuation by patchy vegetation. Acta Oceanologica Sinica, 39(5): 105–114, doi: 10.1007/s13131-020-1572-6

Zhou Xiaoyan, Dai Zhijun, Pang Wenhong, et al. 2022. Wave attenuation over mangroves in the Nanliu Delta, China. Frontiers in Marine Science, 9: 874818, doi: 10.3389/fmars.2022.874818

Zheng Jinhai, Xu Wei, Tao Aifeng, et al. 2023. Synergy between coastal ecology and disaster mitigation in China: Policies, practices, and prospects. Ocean & Coastal Management, 245: 106866, doi: https://doi.org/10.1016/j.ocecoaman.2023.106866

Appendix A: A summary of laboratory tests used in SWAN-CWV model validation

The data from the flume experiments conducted by Hu et al. (2014) was utilized for validating the SWAN-CWV model. A total of 314 tests were carried out, considering three different mimic stem densities, two water depths, and various current-wave conditions (Table A1).

Table A1. Test conditions with different combinations of hydrodynamic conditions (Hu et al., 2014)

Water depth (h)/ vegetation height/m	Wave height (H) /m	Wave period (T)/s	Wave case name	Current velocity (U_c) /(m·s^{-1})
0.25/0.36	0.04	1.0	wave0410[1)]	0/0.05/0.15/0.20
	0.04	1.2	wave0412	0/0.05/0.15/0.20
	0.06	1.0	wave0610	0/0.05/0.15/0.20
	0.06	1.2	wave0612	0/0.05/0.15/0.20
	0.08	1.2	wave0812	0/0.05/0.15/0.20
	0.08	1.5	wave0815	0/0.05/0.15/0.20
	0.10	1.5	wave1015	0/0.05/0.15/0.20
0.50/0.36	0.04	1.0	wave0410	0/0.05/0.15/0.20/0.30
	0.06	1.2	wave0612	0/0.05/0.15/0.20/0.30
	0.08	1.4	wave0814	0/0.05/0.15/0.20/0.30
	0.10	1.6	wave1016	0/0.05/0.15/0.20/0.30
	0.12	1.6	wave1216	0/0.05/0.15/0.20/0.30
	0.12	1.8	wave1218	0/0.05/0.15/0.20/0.30
	0.15	1.6	wave1516	0/0.05/0.15/0.20/0.30
	0.15	1.8	wave1518	0/0.05/0.15/0.20/0.30
	0.15	2.0	wave1520	0/0.05/0.15/0.20/0.30
	0.18	2.2	wave1822	0/0.05/0.15/0.20/0.30
	0.20	2.5	Wave2025	0/0.05/0.15/0.20/0.30

Note: [1)]The case name represents the combination of incident wave height 0.04 m and wave period 1.0 s, namely wave0410.

Appendix B: Sensitivity analysis of SWAN-CWV model grid size

Sensitivity analysis was performed to investigate the impact of different grid sizes on the simulation results for both the modeling of flume experiments (Fig. B1) and field observations (Fig. B2).

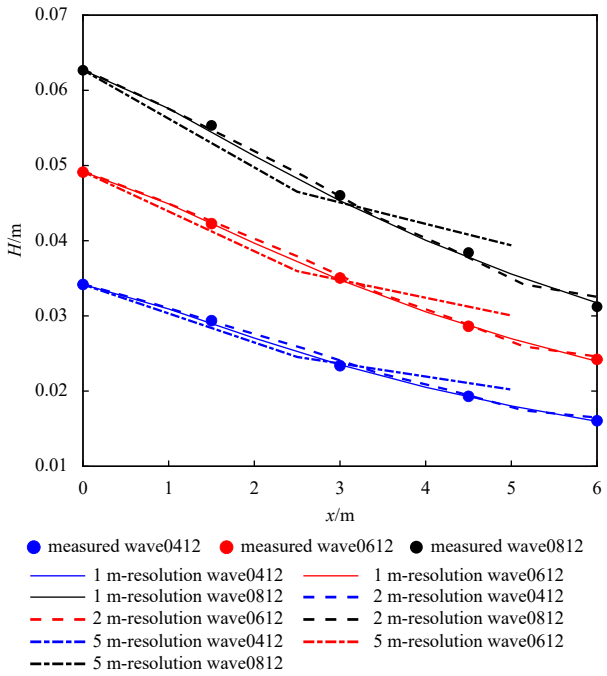

Fig. B1. Sensitivity analysis of the different grid sizes (1 m, 2 m and 5 m) on the SWAN-CWV modeled wave height attenuation by vegetation in the current-wave flows (U_c = 0.20 m/s). All cases are in non-submerged canopies with medium mimic stem densities (139 stems/m^2). The case name stands for the combination of incident wave height 0.04 m and wave period 1.2 s, namely wave0412.

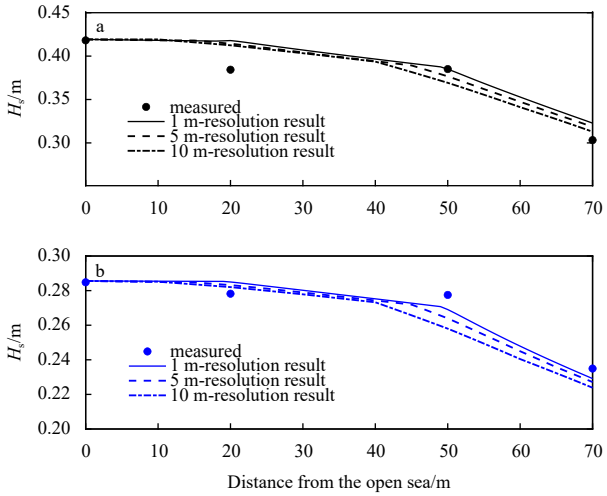

Fig. B2. Sensitivity analysis of the different grid sizes (1 m, 5 m, and 10 m) on the SWAN-CWV modeled wave height attenuation by vegetation in the current-wave flows in Hailing Island: a. U_c= 0.052 m/s, b. U_c= 0.065 m/s.

We preformed sensitivity analyses to show how the grid resolution influences the model outputs (Fig. B1). We chose 1 m, 2 m and 5 m as the model resolution respectively due to the 6-m long vegetation patch in the flume setup. The simulation results of 1 m and 2 m grid sizes are almost the same in all cases (wave 0412, wave 0612, and wave 0812), which are in-line with the measured data (Hu et al., 2014). When the grid size was increased by 5 m, the attenuation of wave height is reduced by nearly 18% compared with other tests with different resolutions. This is because the length of the vegetation area was 5 m, which was inconsistent with the flume settings (the length of the vegetation area was 6 m). Overall, the results show that the grid size does not affect the modeling results provided that the grid size is not too coarse for the flume experiments.

Since the transect in the Hailing Island was 70-m long, we set the sizes of the model grid as 1 m, 5 m, and 10 m respectively. The comparisons of wave evolution in SWAN-CWV model with different resolutions and the field experiment results were shown in Fig. B2. Two cases of the field observations were simulated (H_s = 0.42 m, T_p = 3.3 s, U_c = 0.052 m/s, Fig. B2a; H_s = 0.29 m, T_p = 2.7 s, U_c = 0.065 m/s, Fig. B2b). Overall, the field simulation reaches the same conclusion with the flume simulation results, which is that the grid resolution has little effects on the model outputs.